Open volume defects in ultra-thin TiO2 layers embedded in VMCO-like samples studied with positron annihilation spectroscopy

Khanam, Afrina

2022-06-28

Khanam , A , Slotte , J , Tuomisto , F , Subhechha , S , Popovici , M & Kar , G S 2022 , '
Open volume defects in ultra-thin TiO2 layers embedded in VMCO-like samples studied with
positron annihilation spectroscopy ' , Journal of Applied Physics , vol. 131 , no. 24 , 245301 . https://doi.org/10.1063/5

http://hdl.handle.net/10138/349674
https://doi.org/10.1063/5.0094558

unspecified
acceptedVersion

Open volume defects in ultra-thin TiO_2 layers embedded in VMCO-like samples studied with Positron Annihilation Spectroscop

Afrina Khanam,[1, a)] Jonatan Slotte,[1, 2] Filip Tuomisto,[2] Subhali Subhechha,[3] Mihaela Popovici,[3] and Gouri Sankar Kar[3]

[1)] *Department of Applied Physics, Aalto University, P.O. Box 15100, FI-00076 Aalto, Finland*

[2)] *Department of Physics, P.O. Box 43, FI-00014 University of Helsinki, Finland*

[3)] *Imec vzw, Kapeldreef 75, 3001 Leuven, Belgium*

(Dated: 13 September 2022)

Positron annihilation signals from VMCO-like samples, grown by atomic layer deposition at different temperatures are utilized for the characterization of differences in the open volume defects in the TiN/TiO_2/a-Si heterostructures. Doppler and coincidence Doppler mode of positron annihilation spectroscopy combined with a monoenergetic positron beam were used for this study. Differences observed in the Doppler parameters indicate differences in the positron trapping states of the TiO_2 epilayers grown at different temperatures. Furthermore, the coincidence-Doppler results show that these differences cannot be due to intermixing of the TiO_2 and a-Si layers and formation of thin SiO_2 layers at the interface during the growth process. The results indicate that amount of open volume defects in the TiO_2 layer of the VMCO-structure seems to increase with an increase in the growth temperature.

PACS numbers: 61.72.Ji, 68.55.Ln, 68.65.Ac, 78.70.Bj

[a)] Email:afrina.khanam@aalto.fi

I. INTRODUCTION

Characterization of defects in ultra thin epitaxial layers can be a challenge, doing this non-destructively even more so. In heteroepitaxial semiconductor layers, positron annihilation spectroscopy (PAS) allows for a nondestructive sample analysis.[1] Thin layers can be studied by Doppler broadening of the positron annihilation radiation utilizing a mono-energetic positron beam. Low energy positrons ($0 - 3$ keV) can be used to study near-surface layers and thin films[2]. However, as the sample surface can act as a positron trap, positrons implanted at very low energies can annihilate at the surface. Furthermore, interfaces in general, and especially in thin epilayer heterostructure, can be significant positron traps. Nevertheless, with suitable precautions positron parameters of the annihilation radiation can provide information not only on the layer of interest, but also on the interfaces in the layered structure. This information can be crucial for the design, understanding and analysis of the critical physical properties of functional thin-materials and engineered nanostructures.

PAS has previously been utilized for detecting ultra-thin layers embedded in comparatively thicker layers. Hugenschmidt *et al.* and Pikart *et al.* reported on the sensitivity of positrons for ultra thin Sn and Au layers embedded in Al.[3–5]. Positrons were shown to be able to detect a layer of Sn as thin as 0.1 nm embedded below 200 nm:s of Al. This heightened sensitivity was shown to be due to a significant disparity in the positron affinity between Sn and Al.[6] These studies focused on the sensitivity of positrons to a thin layer or a cluster of atoms embedded in a significantly different matrix, mainly metals. Some positron studies on thin epitaxial layers in a superlattice structure, for a more technologically relevant approach, have also been conducted. Nitrogen related vacancy defects were investigated in GaAs based quantum well superlattices, where the well thickness was 6 nm and barrier thickness 30 nm.[7] In a similar type of study point defect influence on Al and Ga interdiffusion in AlSb/GaSb superlattice structures, where the well thickness was 13 nm and barriers 2 - 3 nm.[8] However, in both of these studies the total sample structure was over 100 nm, making the interpretation of the results more straightforward. In an investigation on point defects in HfO_2 thin films of thicknesses of $10 - 100$ nm, Alemany *et al.* found, by applying PAS, higher defect concentrations in atomic layer deposition (ALD) HfO_2/Si layers than in physical vapor deposition (PVD) layers. They also suggested that, open volume defect concentrations depend on the deposition process of the layer.[9]

Thin film based resistive switching random access memories (RRAM) have gained significant attentions and are considered as a promising candidate for the next generation memory applications in terms of scalability, low switching currents, self-rectifying, complimentary metal oxide semiconductor (CMOS) compatibility, low cost, and endurance and retention complimented with simple fabrication process[10–15] Amorphous Si (a-Si) and anatase TiO_2 - based vacancy modulated conductive oxide (a-VMCO) RRAM thin devices are gaining interest due to non-linear *I-V* characteristics with low current, bipolar, and self-compliant switching, since the defect profile modulation takes place only in the TiO_2 switching layer.[14,16] Resistive switching in the TiO_2 layer is modulated by the electrical controlling of the oxygen vacancies (V_O) which creates the a-VMCO active layer.[10,17,18] Therefore, vacancy distribution in the thin switching layer plays an important role in the a-VMCO RRAM devices.

In this work, PAS was applied to VMCO-like samples consisting of 15 nm ultra-thin TiO_2 epilayers grown at different conditions, embedded in a heterostructure of TiN and amorphous SiO_2. A monoenergetic positron beam study shows clear differences between the samples. Coincidence Doppler Broadening spectroscopy was applied to characterize this difference in more detail.

II. EXPERIMENTAL DETAILS

A set of four VMCO-like samples were fabricated, a schematic figure of the grown sample structure is shown in Fig 1. The VMCO-like stack was formed by a 15 nm anatase TiO_2 layer and a 8 nm amorphous Si barrier layer (a-Si), with top and bottom layers of 10 nm TiN.[19] The TiO_2 ultra-thin layers had been deposited by ALD at different temperatures (210, 225, 235 and 250 °C). The a-Si barrier layer was grown by PVD at room temperature (25 °C). A similarly prepared sample with a thicker (50 nm) TiO_2 layer grown at 210 °C was used as a reference sample.

We used a monoenergetic slow positron beam to characterize the samples. A ^{22}Na source combined with a tungsten moderator was used as a positron source. The positrons were electrostatically accelerated and magnetically guided to the sample. When measuring such thin sample structures with PAS, mainly two unavoidable facts influence the measurements and the interpretations of the data, i.e., the positron implantation profile and the positron diffusion. The implantation profile can be described by a derivative of a Gaussian func-

tion[20,21]

$$P(x,E) = \frac{m x^{m-1}}{x_0^m} \mathrm{e}^{-(x/x_0)^m}, \qquad \text{where} \qquad x_0 = \frac{AE^n}{\rho\Gamma\left(1+\frac{1}{m}\right)}. \tag{1}$$

The mean stopping depth is $\bar{x} = AE^n[\mathrm{keV}]$. where E is the positron implantation energy and A, m and n are empirical parameters. A value of 1.6 is commonly used for n.[22] Hence, the width of the implantation profile depends heavily on implantation energy, with an increase in energy resulting in a broader implantation profile. As a consequence, if one wants to characterize positron traps in a single thin layer or at interfaces associated with a thin layer, this layer has to be located fairly close to the sample surface at a depth of approximately 10 - 100 nm. An implantation energy of approximately 1.2 keV corresponds to $\bar{x}$ being in the layer (TiO_2) of interest.

After implantation and stopping, the positron thermalizes within a few ps through ionization, core electron excitation, electron-hole excitation and phonon emission.[1] Thereafter the positron distribution in the sample is governed by diffusion, possible drift due to an electric field and by trapping into defects. The positron diffusion length in a positron trap-free semiconductor is 100 - 200 nm.[1] In an experiment with fast unmoderated positrons, where the implantation profile width is of the order of 50 μm the diffusion broadening of the implantation profile is irrelevant. However, in an experiment with thin film heterostructures or ion implanted/irradiated samples, the positron diffusion can heavily influence the results.

Furthermore, in the presence of defects, positrons may get trapped in the defects before annihilation, which eventually reduces the effective diffusion length. In a sample with a high concentration of point defects $\approx 10^{18}$ cm^{-3}, the effective diffusion length can be of the order of 10 nm. Nevertheless, for positrons implanted with an energy of a few keV, the width of the positron implantation profile will be of the same order of magnitude as the mean implantation depth (10 - 40 nm). Hence, the positron diffusion will either heavily influence the depth profile of the annihilating positrons (high point defect concentration) or completely dominate it (low point defect concentration). In an epitaxial heterstructure, the interfaces between layers will, irrespective of point defects, heavily influence the PAS experiment.

After implantation and thermalization, the positrons annihilate with electrons either in a delocalized state in the lattice or trapped in a defect, resulting in the emission of two γ-quanta with energies of 511 keV. The momentum of the annihilating electron-positron

pair causes a Doppler shift in the annihilation radiation as the energy and momentum are conserved in the annihilation process. Hence, the annihilation line is broadened, mainly due to the momentum of the annihilating electron. A more detailed discussion on the Doppler broadening PAS technique is presented in Refs.[1,23,24].

Doppler broadening spectroscopy (DOBS) measurements, referred to as normal-Doppler, were conducted using a high purity Ge detector (HPGe) with a resolution of 1.3 keV at 511 keV. Approx. 10^6 annihilation events per spectrum were collected. The energies of the monoenergetic positrons were varied from 0.2 to 25 keV. Two shape parameters, conventionally designated as the S- and W -parameters were used to characterize the spectra. The low momentum valence parameter S, describing annihilations mainly with valence electrons, is the ratio of counts in the central region of the annihilation line to the total counts of the broadened line. The second parameter, the high momentum parameter W, is the ratio of counts in the wing region of the annihilation line to the total counts of the broadened line.[23] The W parameter describes annihilation mainly with core electrons. The S integration energy window was set as $|p_L| < 0.46$ a.u., whereas the W integration window was 1.6 a.u. $< |p_L| < 3.9$ a.u. Here, a.u. signifies atomic units. An increase (decrease) in the S (W) parameter compared to a defect free reference usually indicates the existence of open volume (vacancy) defects.

The measured annihilation parameters S and W are superpositions of the parameters for the different annihilation states in the lattice.[23]

$$S = \eta_B S_B + \sum_i \eta_{Di} S_{Di} \qquad \text{and} \qquad W = \eta_B W_B + \sum_i \eta_{Di} W_{Di} \tag{2}$$

Here, η_B is the fraction of positrons annihilating in the bulk state, and η_{Di} is the fraction of positrons annihilating in the defect state i. S_B (W_B) and S_{Di} (W_{Di}) are the bulk and defect parameters, respectively. If a sample contains only two annihilation states, the $W(S)$-plot of the measurement forms a segment of a line between these states, *e.g.*, bulk and defect states. A deviation from the line between the defect and bulk state indicates that positrons annihilate in more than two annihilation states.

2D-coincidence Doppler broadening spectroscopy (CDOBS), referred to as coincidence-Doppler is an efficient technique to identify vacancy defects and the chemical surroundings of vacancies in the case of vacancy-complexes. After completion of normal-Doppler experiments, coincidence-Doppler measurements were done in order to deepen the understanding

of the annihilation states in the thin epitaxial heterostructure. The resolution of the two detector HPGe system in the coincidence set-up was 1.0 keV at 511 keV. A positron implantation energy of 1.2 keV was used to maximize annihilation in the TiO_2 epilayer for the CDOBS measurements. Approx. 12×10^6 counts for a single spectrum were collected in this experiment. A 50 nm thick TiO_2 reference sample was used for normalization of the data.

III. RESULTS

Figure 2 shows the Doppler shape parameters as a function of positron implantation energy for the samples of interest and for the reference sample. Although the data from the reference sample is elongated on the energy scale, due to a thicker TiO_2 layer, the similar shapes of the sample- and reference data suggest that the structure can indeed be characterized with PAS. The S- and W- parameter values at $\sim$ 1.2 keV (minimum in S parameter, maximum in W parameter in the sample data) correspond to annihilations where a majority of the annihilation events take place in the TiO_2 layer, although a non-negligible fraction of positrons end up annihilating at the TiO_2−a-Si interface and in the a-Si underneath. Also the TiN/TiO_2 interface could contribute. Slight differences in the S- and W-parameters are seen for the TiO_2 epilayers at $\sim$ 1.2 keV.

Figure 3 presents the core annihilation parameter W as a function of the valance annihilation parameter S for all samples and the reference. As can be observed, the surface annihilation states, assumed here to be equal to the values for the lowest positron implantation energy, are very similar for the 210 °C, 235 °C and 250 °C samples. The 225 °C sample has a slightly higher S value at the surface. Hence, we can conclude that the differences in the shape parameters observed for the TiO_2 layers (at $\sim$ 1.2 keV) arise from small differences in the annihilation environment for the positrons.

Figure 4 shows the CDOBS results for the the VMCO-like epilayers grown at different temperatures scaled to the TiO_2 reference sample. For comparison, the inset shows the momentum distribution for a thick SiO_2 sample. As can be observed, the VMCO-like samples follow the same trends as in Fig. 3. Furthermore, there is a clear difference in comparison to the thick TiO_2 reference sample. For the reference sample the data is collected more or less exclusively from the TiO2 layer, since the width of the depth profile of the annihilating positrons (implantation + diffusion broadening) is less than the width of the layer. For all

samples, the intensity at high momenta is clearly lower than the reference (1.00) and higher at low momenta. A similar trend is seen in the spectrum for the SiO_2 sample. As TiO_2 layer in the VMCO-like samples is grown on top of an amorphous Si layer, there is expected to be an intermixing of the two layers during the growth process and the a formation of SiO_2 at the interface. However, as will be discussed in the next section, the difference between the VMCO-like samples and the reference sample cannot be explained solely by a superposition between annihilation in SiO_2 and TiO_2.

IV. DISCUSSION

The DOBS results of Figs. 2 and 3 indicate a slight difference between the the TiO_2 layers grown at different temperatures. A closer look reveals that the sample grown at the highest temperature (250 °C) has the highest (lowest) S-(W)-value in the layer of interest (TiO_2) and that the sample grown at the lowest temperature (210 °C) has the lowest (highest) S-(W)-value, respectively. As a higher S-parameter typically indicates more open volume for the positron wavefunction to be confined in, this could indicate more open volume defects with increasing growth temperature. However, as differences in growth temperatures also could result in differences in the intermixing of the a-Si and the TiO_2 layers, this difference in annihilation parameters could also be explained by how much SiO_2 is formed next to the TiO_2 layer.

Fig. 4 shows a similar shape for the momentum ratio distributions for all the VMCO-like samples. This suggest that the annihilation states for the positrons is similar in the different samples, albeit with slightly different annihilation fractions and clearly different than the 50 nm thick TiO_2 reference sample. As can be seen from the inset in Fig. 4, the momentum distribution for the SiO_2 reference is clearly more narrow than that for the TiO_2 reference, i.e., $I_{SiO_2}/I_{TiO_2} > 1$ at low momenta and $I_{SiO_2}/I_{TiO_2} < 1$ at high momenta. Visually this appears to be true also when comparing SiO_2 to the VMCO-like samples.

In mathematical terms, if the differences between the VMCO-like samples would only be due to differences in how the a-Si is oxidized at different temperatures, the measured spectrum could be explained by the simple equation

$$\mathrm{Spec} = \eta_{TiO_2}\mathrm{Spec}_{TiO_2} + \eta_{SiO_2}\mathrm{Spec}_{SiO_2}. \quad (3)$$

In Eq (3) Spec_{TiO_2} and Spec_{SiO_2} are the reference spectra, and η_{TiO_2} and η_{SiO_2} are the

annihilation fractions, respectively. The annihilation fractions are related by the simple relation

$$\eta_{SiO_2} = 1 - \eta_{TiO_2}. \tag{4}$$

Hence, this superimposed spectrum (Eq (3)) contains only one free parameter. Figure 5 shows a representative set of experimental and superimposed (fitted) intensity ratios. As can be seen the simple superposition in Eq. (3) does not explain the differences between the TiO_2 reference and the VMCO-like samples. As expected the superimposed spectrum is too narrow and the shoulder around 1 a.u., i.e. the momentum region between the S and W parameters, cannot be explained by a superposition of the TiO_2- and SiO_2 reference spectra.

Although we are able to make conclusions on the origin of the annihilation signal in such thin sample layers, we should also emphasize that there are both additional limitations and advantages for making conclusions on defects in these VMCO-like samples. The main limitation for making conclusions on the nature of the positron traps in the TiO_2 layers is the lack of a thick defect free TiO_2 reference. It is likely that the TiO_2 reference used in this study contains positron traps. Hence, this makes identification and quantification of the open volume defects in practice impossible, and only differences between the samples could be characterized. This drawback applies to PAS studies in general, not only to ultra thin layers. A clear advantage for characterizing the VMCO-like samples, was the apparent differences in the possible annihilation states in the samples, shown in Figs. 3 and 4. Hence, the 15 nm TiO_2 layer could be distinguished from the surface, TiN and SiO_2 layers.

We can therefore conclude that the differences between the VMCO-like samples observed both in the DOBS and the CDOBS measurements are due to differences in the open volume defects, more precisely due to differences in open volume defects in the TiO_2 layer of the VMCO structure. As the intensity at low momenta and consequently also the S-parameter are indicative of the amount of open volume defect and/or their size, it seems as a higher growth temperature results in more open volume defects in the TiO_2 layer.

V. SUMMARY

In conclusion, we have demonstrated that the Doppler broadening and the coincidence Doppler broadening mode of PAS combined with a monoenergetic positron beam, with a suitable positron implantation energy, can be applied to study ultra thin technologically

relevant samples. The slight differences in the annihilation signals from the TiO_2 layer of the VMCO-like structure indicate that a higher growth temperature for the TiO_2 layer results in more open volume defects.

VI. ACKNOWLEDGEMENTS

One of the authors (Afina Khanam) acknowledges Tekniikan edistämissäätiö for the financial support.

REFERENCES

[1]J. Slotte, I. Makkonen, and F.Tuomisto, *Characterisation and Control of Defects in Semiconductors* (IET, London, 2019) edited by F. Tuomisto.

[2]K. Saarinen, P. Hautojärvi, and C. Corbel, *Identification of Defects in Semiconductors* (Academic Press, New York, 1998) edited by M. Stavola.

[3]C. Hugenschmidt, P. Pikart, M. Stadlbauer, and K. Schreckenbach, Phys. Rev. B **77**, 092105 (2008).

[4]P. Pikart, C. Hugenschmidt, J. Mayer, M. Stadlbauer, and K. Schreckenbach, Appl. Surf. Sci. **255**, 245 (2008).

[5]P. Pikart and C. Hugenschmidt, Phys. Rev. B **84**, 014106 (2011).

[6]M. J. Puska and R. M. Nieminen, J. Phys. Condens. Matter **1**, 6081 (1989).

[7]J. Slotte, K. Saarinen, E.-M. Pavelescu, T. Hakkarainen, and M. Pessa, Appl. Phys. Lett. **89**, 061903 (2006).

[8]J. Slotte, T. F. K. M. Gonzalez-Debs, and J. G. Cederberg, J. Appl. Phys. **102**, 023511 (2007).

[9]M. Alemany, A. Chabli, E. Oudot, F. Pierre, P. Desgardin, F. Bertin, M. Gros-Jean, and M. F. Barthe, Journal of Physics: Conference Series **791**, 012019 (2017).

[10]D. H. Kwon, K. M. Kim, J. H. Jang, J. M. Jeon, M. H. Lee, G. H. Kim, X.-S. Li, G. S. Park, B. Lee, S. Han, M. Kim, and C. S. Hwang, Nature Nanotechnology **5**, 148–153 (2010).

[11]S. Larentis, F. Nardi, S. Balatti, D. C. Gilmer, and D. Ielmini, IEEE Transactions on Electron Devices **59**, 2468–2475 (2012).

[12]H. P. Wong, H. Lee, S. Yu, Y. Chen, Y. Wu, P. Chen, B. Lee, F. T. Chen, and M. Tsai, Proceedings of the IEEE **100**, 1951–1970 (2012).

[13]C.-W. Hsu, I.-T. Wang, C. L. Lo, M.-C. Chiang, W. Y. Jang, C.-H. Lin, and T.-H. Hou, 2013 Symposium on VLSI Technology , T166–T167 (2013).

[14]B. Govoreanu, D. Crotti, S. Subhechha, L. Zhang, Y. Y. Chen, S. Clima, V. Paraschiv, H. Hody, C. Adelmann, M. Popovici, O. Richard, and M. Jurczak, "A-vmco: A novel forming-free, self-rectifying, analog memory cell with low-current operation, nonfilamentary switching and excellent variability," *2015 Symposium on VLSI Technology*, , T132–T133 (2015).

[15]X. Xu, Q. Luo, T. Gong, H. Lv, S. Long, Q. Liu, S. S. Chung, J. Li, and M. Liu, "Fully cmos compatible 3d vertical rram with self-aligned self-selective cell enabling sub-5nm scaling," *2016 IEEE Symposium on VLSI Technology*, , 1–2 (2016).

[16]J. Ma, Z. Chai, W. Zhang, B. Govoreanu, J. F. Zhang, Z. Ji, B. Benbakhti, G. Groeseneken, and M. Jurczak, 2016 IEEE International Electron Devices Meeting (IEDM) , 21.4.1–21.4.4 (2016).

[17]D. B. Strukov, G. S. Snider, D. R. Stewart, and R. S. Williams, Nature **453**, 80–83 (2008).

[18]S. Park, B. M. Köpe, and Y. Nishi, IEEE Electron Device Letters **32**, 197–199 (2011).

[19]M. Popovici, J. Swerts, K. Tomida, D. Radisic, M.-S. Kim, B. Kaczer, O. Richard, H. Bender, A. Delabie, A. Moussa, C. Vrancken, K. Opsomer, A. Franquet, M. A. Pawlak, M. Schaekers, L. Altimime, S. V. Elshocht, and J. A. Kittl, Phys. Status Solidi **5**, 19 (2011).

[20]S. Valkealahti and R. M. Nieminen, Appl. Phys. A **35**, 51 (1984).

[21]A. F. Makhov, Sov. Phys. Sol. State **2**, 1934 (1961).

[22]A. Vehanen, K. Saarinen, P. Hautojärvi, and H. Huomo, Phys. Rev. B **35**, 4606 (1987).

[23]F. Tuomisto and I. Makkonen, Rev. Mod. Phys. **85**, 1583 (2013).

[24]R. Krause-Rehberg and H. S. Leipner, *Positron Annihilation in Semiconductors* (Springer, Berlin, 1999).

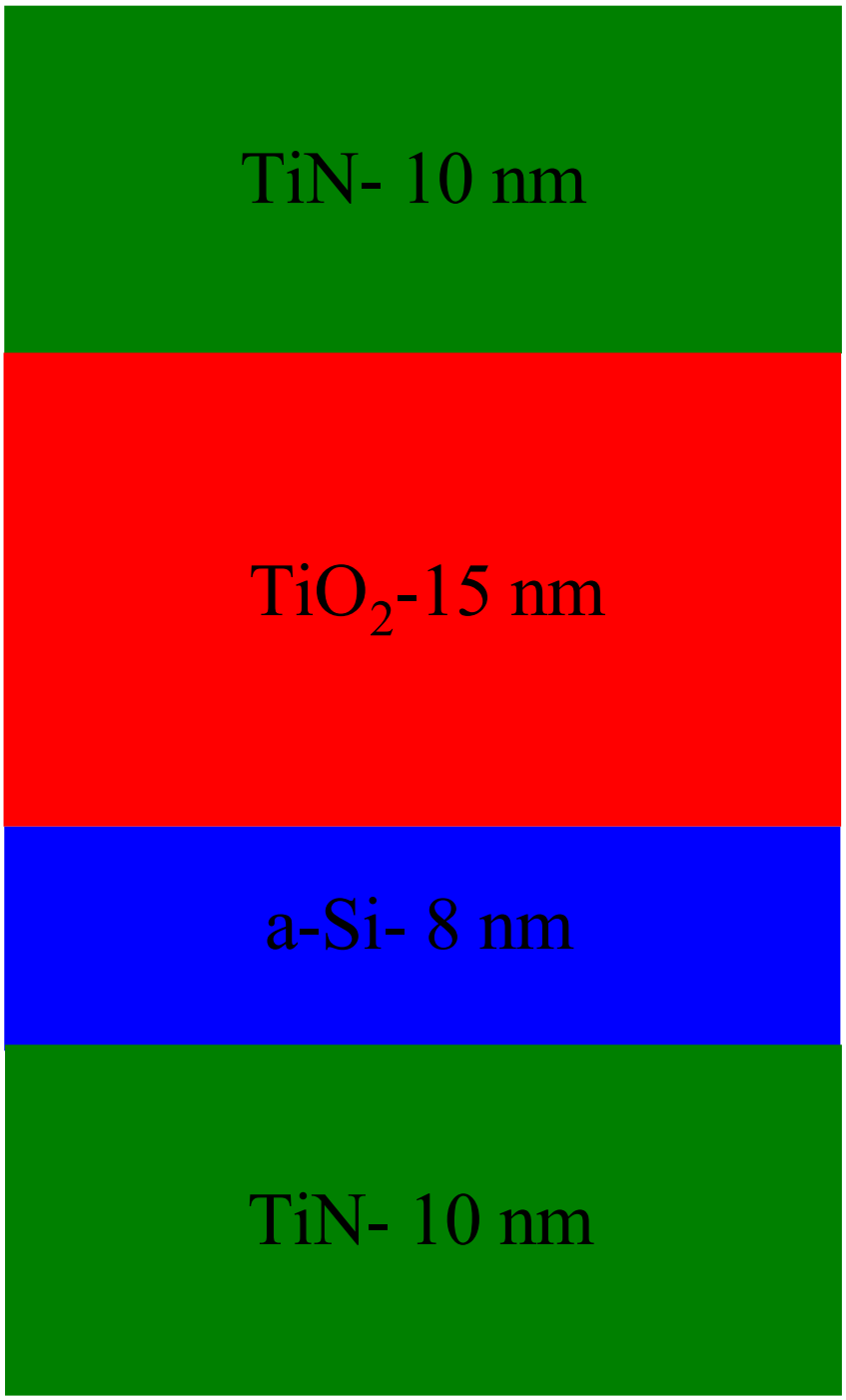

FIG. 1. Schematic presentation of the sample structure.

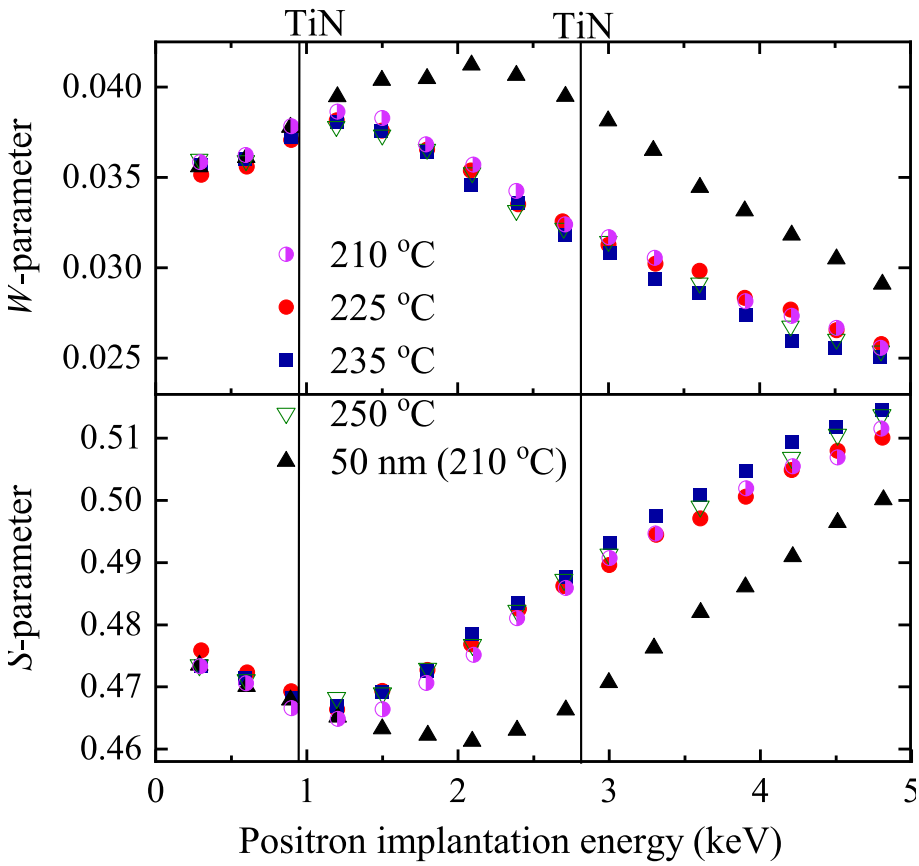

FIG. 2. $W(E)$ and $S(E)$ plots for the VMCO samples. The indicated temperature is the growth temperatures of the TiO_2 layers. The vertical lines in the figure indicate where the positron mean implantation depth coincides with TiN/TiO_2 and a-Si/TiN interfaces (see Fig. 1). The errors in the two parameters are $\Delta S = 5 \times 10^{-4}$ and $\Delta W = 1.5 \times 10^{-4}$, respectively.

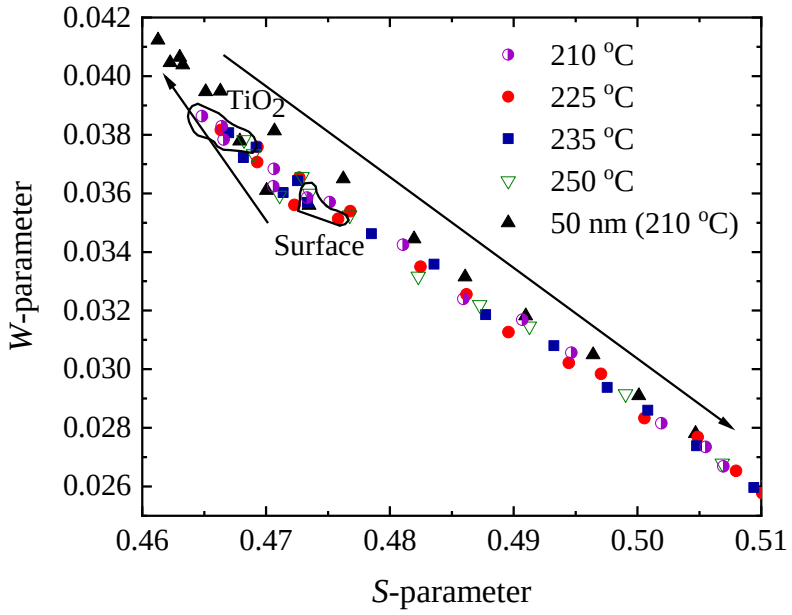

FIG. 3. The $W(S)$ plot for different samples with different growth temperature. The annihilation states for the TiO_2 layer and the surface are indicated in the VMCO-like samples. The arrows indicate increasing positron implantation energies.

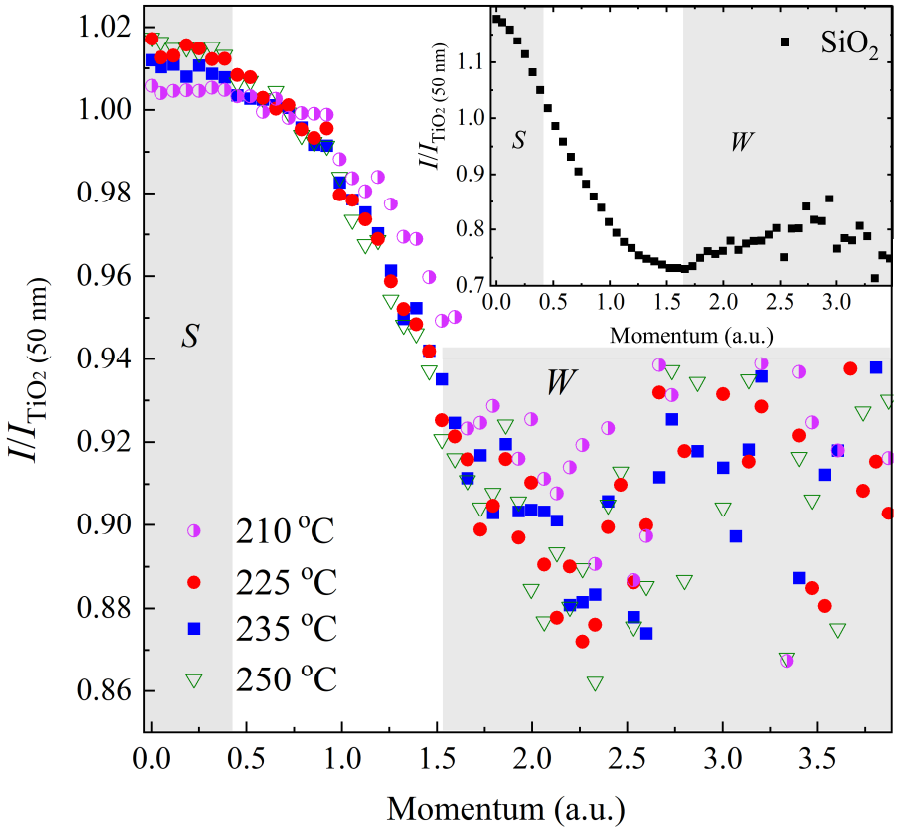

FIG. 4. Intensity ratio for different samples measured with CDOBS. The spectra were normalized to the spectrum from the 50 nm TiO_2 reference. The inset shows the intensity ratio for a SiO_2 reference sample. The S- and the W-parameter windows are indicated with the shaded regions.The positron implantation energy for the samples was chosen as 1.2 keV.

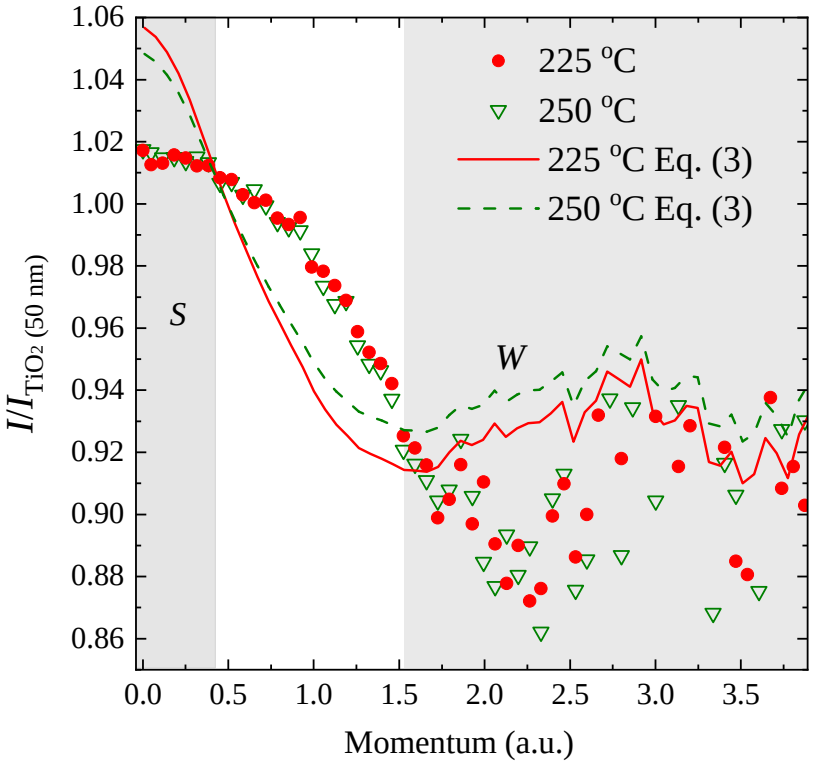

FIG. 5. Experimental and superimposed (Eq. (3)) intensity ratios for a representative sample set. The sample spectra were normalized to the spectrum from the 50 nm TiO_2 reference.